JOURNAL OF GEOPHYSICAL RESEARCH, VOL. 89, NO. A3, PAGES 1683–1694, MARCH 1, 1984

F Layer Ionization Patches in the Polar Cap

E. J. WEBER[1], J. BUCHAU[1], J. G. MOORE[1], J. R. SHARBER[2], R. C. LIVINGSTON[3], J. D. WINNINGHAM[4], AND B. W. REINISCH[5]

Ground-based optical and digital ionosonde measurements were conducted at Thule, Greenland to measure ionospheric structure and dynamics in the nighttime polar cap *F* layer. These observations showed the existence of large-scale (800–1000 km) plasma patches drifting in the antisunward direction during a moderately disturbed ($Kp \geq 4$) period. Simultaneous Dynamics Explorer (DE-B) low-altitude plasma instrument (LAPI) measurements show that these patches with peak densities of $\sim 10^6$ el cm^{-3} are not locally produced by structured particle precipitation. The LAPI measurements show a uniform precipitation of polar rain electrons over the polar cap. The combined measurements provide a comprehensive description of patch structure and dynamics. They are produced near or equatorward of the dayside auroral zone and convect across the polar cap in the antisunward direction. Gradients within the large scale, drifting patches are subject to structuring by convective instabilities. UHF scintillation and spaced receiver measurements are used to map the resulting irregularity distribution within the patches.

1. INTRODUCTION

In addition to solar ionization, polar cap *F* layer structure is controlled by direct precipitation of low-energy electrons and by plasma convection. As outlined by *Kelley et al.* [1982], these are also controlling factors for the generation, transport, and decay of ionospheric irregularities that exist over a wide range of scale sizes in the polar region.

Previous coordinated measurements in the polar cap [*Weber and Buchau*, 1981] have shown the structure and drift of subvisual *F* layer auroras. They are noon-midnight aligned, drift predominately in the dawn to dusk direction and are produced by fluxes of low-energy ($E < 500$ eV) electrons. Intense ionospheric irregularities within the auroral arcs cause amplitude and phase fluctuations (scintillation) on satellite to ground UHF radio transmissions and spread *F* on the ionosonde high-frequency echo returns.

In a recent study, *Hardy* [1983] has classified types of electron fluxes precipitating into the polar cap. His class III spectra (accelerated through a field aligned potential gradient from 50 V to 2 kV) are most clearly associated with the observed ionospheric characteristics of the subvisual *F* layer arcs. They are the polar showers reported by *Winningham and Heikkila* [1974]. An important result from the satellite measurements of *Hardy* [1983] is the strong dependence on the occurrence of electron fluxes in the polar cap with the north-south component of the interplanetary magnetic field (B_z). A positive correlation exists between the presence (absence) of accelerated electron fluxes above polar rain energy in the polar cap with northward (southward) B_z. The occurrence of more intense (visible) auroras, measured by all-sky cameras [*Lassen and Danielsen*, 1978] and by the DMSP satellite imager [*Gussenhoven*, 1982] also show a positive correlation with northward B_z. Thus, during times of northward B_z, and statistically during quiet geomagnetic conditions as measured by *Kp* and *AE* [*Maezawa*, 1978], accelerated polar rain electrons (polar showers) precipitate into the polar cap and produce *F* layer auroras and associated ionospheric irregularities. UHF scintillation measurements, which are a measure of kilometer scale irregularities, do not, however, show a strong dependence on the level of geomagnetic activity. Scintillation occurrence measured from Thule, Greenland (86° corrected geomagnetic latitude (CGL)), was shown by *Aarons et al.* [1981] to be essentially independent of *Kp*. Thus, during disturbed geomagnetic periods, when structured particle precipitation into the polar cap does not directly produce the observed irregularities, transport of plasma (and irregularities) from other production regions must be considered.

The purpose of this paper is to describe large-scale (~ 1000 km) plasma patches observed in the polar cap during a moderately disturbed ($Kp \geq 4$) period. The patches, observed by optical and radio techniques, are convected in the antisunward direction across the central polar cap from a source region near the dayside auroral oval. UHF scintillation and spaced receiver measurements provide an estimate of irregularity intensity and drift velocity. Simultaneous Dynamics Explorer (DE-2) low-altitude plasma instrument (LAPI) measurements show a uniform precipitation of polar rain; regions of accelerated and structured low-energy electron precipitation were not observed.

Recently, *Kelley et al.* [1982] have incorporated many of the observed features of high-latitude irregularities in a convection/decay model. The results of this study, and those of *Weber and Buchau* [1981] on direct irregularity production, will improve irregularity source functions in future models.

2. OBSERVATIONS

Polar cap ionospheric measurements were conducted from Thule Air Base, Greenland (76.5°N, 68.7°W, 86° CGL), from January 17–27, 1982. The objectives of these experiments were to measure optical and radio wave signatures of polar cap ionospheric structures, to relate these to in situ measurements from the Dynamics Explorer satellite, and to determine the relation of the large-scale plasma structures to small-scale (kilometer) irregularities through satellite-ground scintillation measurements.

2.1. *Optical Measurements*

Optical measurements were performed by using a wide angle (155° field of view) all-sky imaging photometer (ASIP)

[1] Ionospheric Physics Branch, Air Force Geophysics Laboratory.
[2] Physics and Space Sciences Department, Florida Institute of Technology.
[3] Radio Physics Laboratory, SRI International.
[4] Southwest Research Institute.
[5] Center for Atmospheric Research, University of Lowell.

Paper number 3A1459.

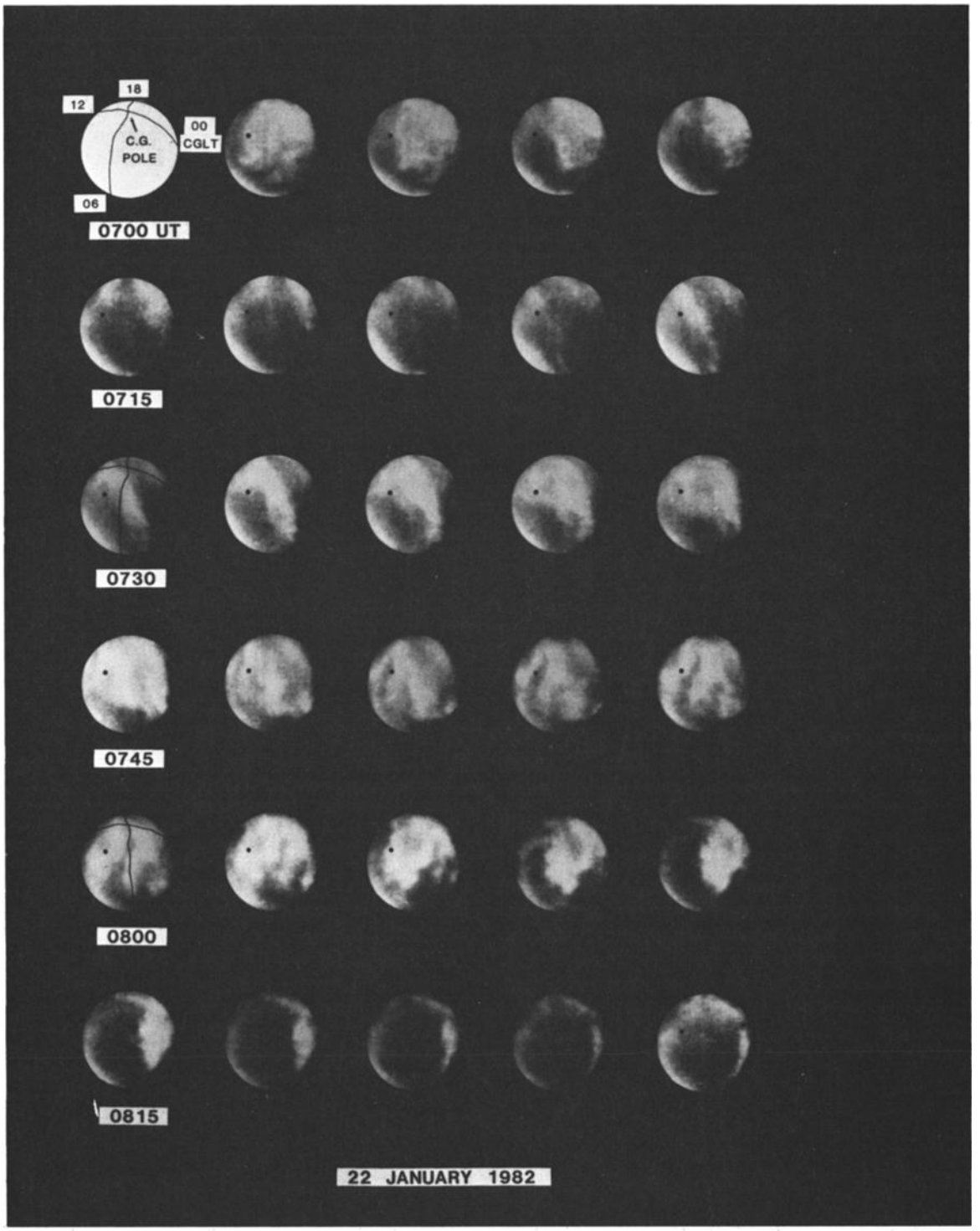

Fig. 1*a*. Sequence of 6300-Å all-sky images at 3-min intervals from 0703 to 0827 UT, January 22, 1982, from Thule, Greenland (86° CGL). The dawn-dusk (06–18) and noon-midnight (12–00) CG local time meridians were projected into the images at a height of 250 km. The intersection of the two meridians is the north CG pole, which is at the top of each image. The dot represents the direction to the polar orbiting beacon satellite used for the 250-MHz scintillation measurements.

[*Weber et al.*, 1977] with interference filters to measure 6300 Å and 7774 Å O I, 4278 Å N_2^+ and 5200 Å N I. A sequence of 6300 Å ASIP images, at 3-min intervals, from 0700 to 1127 UT, January 22, 1982, is shown in Figures 1*a–c*. The images were made by using a 30-s integration time and cover a dynamic range of ~20–400 R. For an assumed emission height of 250 km, the total image diameter is ~1600 km (lens vignetting reduces the useful diameter to ~1200 km). For spatial reference, the dawn-dusk (06–18) and noon-midnight (12–00) corrected geomagnetic (CG) meridians are projected into the images for a height of 250 km. The intersection of these meridians is the north CG pole, which is located toward the top of each image.

The images show structured 6300-Å emission in the form of

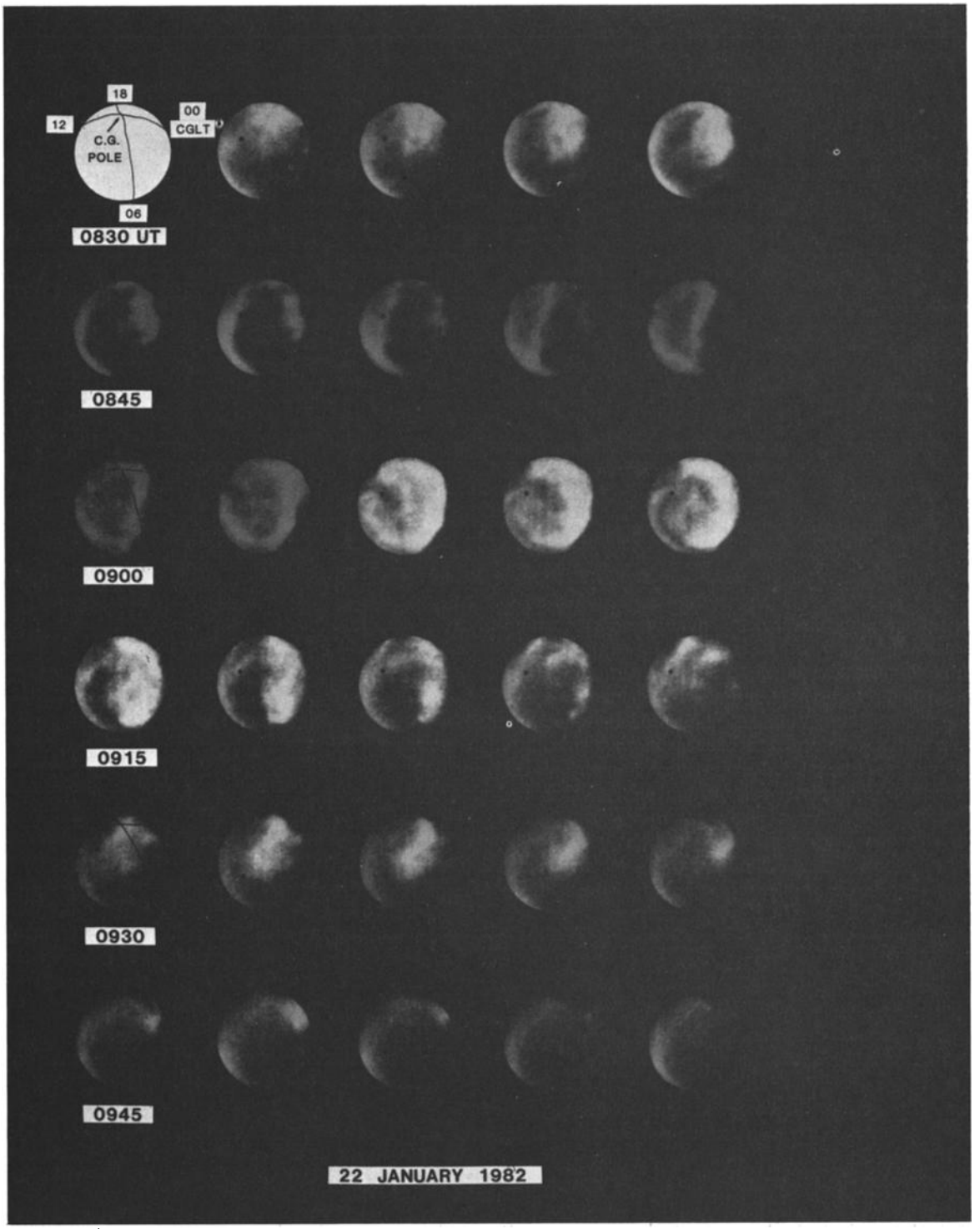

Fig. 1*b*. Same as Figure 1*a* for 0833 to 0957 UT.

~800- to 1000-km diameter patches, and dawn-dusk elongated features drifting in the antisunward direction. Patches are observed near the zenith at 0706, 0806, 0933, 1030, and 1112 UT. Two dawn-dusk elongated features drifted through the zenith at 0730 and 0857 UT. Both types of structures drift in the antisunward direction, first appearing on the noon horizon and disappearing beyond the midnight horizon of the ASIP. During this period, drift velocities ranged from 500 to 1000 m s^{-1}. These speeds are similar to previously reported antisunward plasma drifts measured by AE-C [*Heelis and Hanson*, 1980] and with $E \times B$ drift velocities derived from electric field measurements [*Heppner*, 1972]. The images in Figure 1 show a steady glow on the noon horizon near 79° CGL. This is the high latitude edge of the auroral oval in the 06–10 CGLT sector.

The all-sky images provide a measure of the large-scale structure and drift of the 6300-Å emission features over a 1200-km region in the polar cap for a comparison with other remote and in situ measurements. To illustrate the quantitative behavior of the optical emission, the 6300-Å zenith inten-

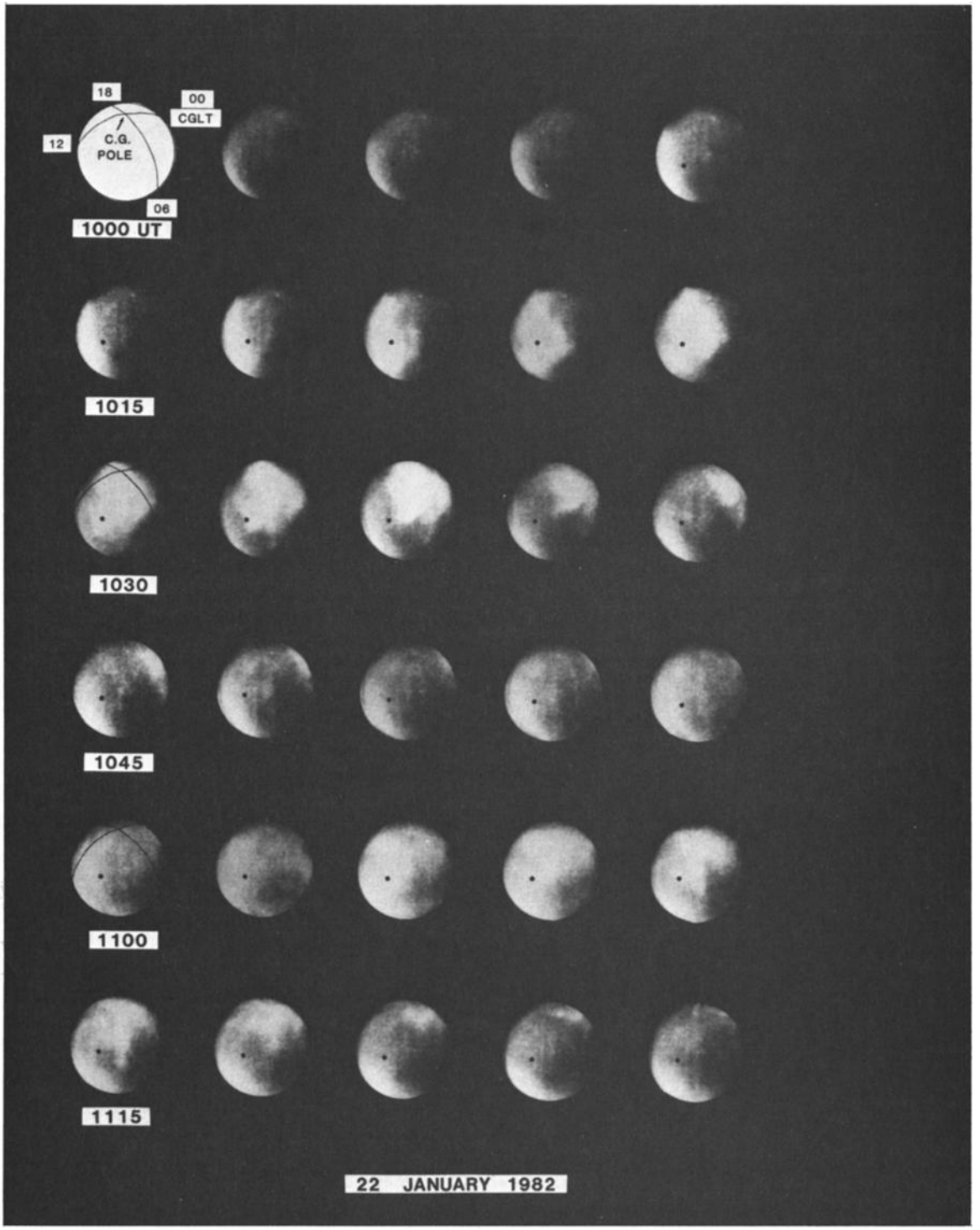

Fig. 1c. Same as Figure 1a for 1003 to 1127 UT.

sity measured by a 1-m Ebert-Fastie spectrometer is shown in Figure 2. The 6300-Å emission reached maximum values of 200–300 R within the patches and decreased to 70–100 R in the background ionosphere. The 3914-Å N_2^+ emission was also measured. This did not vary from outside to inside the patches and showed only a gradual increase with increasing CGLT. The intensity variations will be used in section 2.3 to separate polar rain excitation (aurora) from the dissociative recombination (airglow) contribution to the total measured 6300-Å intensity.

2.2. *Ionosonde Measurements*

Ionospheric soundings were performed by using a Digisonde 128 PS [*Bibl and Reinisch*, 1978] operated at a rate of one ionogram every 2.5 min. The Digisonde 128 PS provides the standard virtual height versus frequency (or $h'f$) information, the amplitudes of the returned signals and of special significance for measurements in a highly structured and dynamic environment, the predominant Doppler shift in each frequency range bin. During these experiments the Digisonde

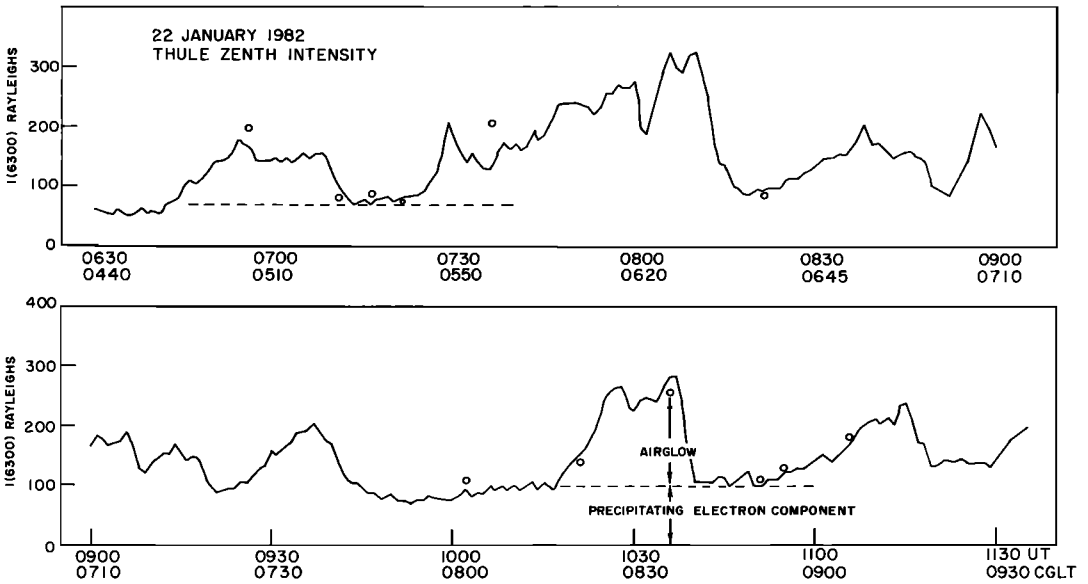

Fig. 2. 6300-Å zenith intensity from Thule, Greenland from 0630 to 1135 UT, January 22, 1982. Also shown are calculated intensities from precipitating electrons (dashed line) and from the combined precipitating electron and dissociative recombination components (open circles).

was operated in a mode to perform Doppler shift measurements over a range of ± 22 Hz. This Doppler capability allows identification and tracking of drifting F region irregularity structures in the presence of spread F. The processing techniques developed for analysis of the Doppler ionograms collected during the January 1982 Polar Cap Campaign have been reported by *Buchau et al.* [1983]. Their analysis showed a positive correlation between bulk drift velocity of polar cap structures and geomagnetic activity (Kp) as well as excellent agreement between instantaneous drift measurements based on the Doppler shift and the bulk velocities derived from optical imaging data. Of importance to this study is the capability of separating spread F ionograms into two subionograms that individually display returns from approaching and receding structures and/or scatterers. A sequence of selected ionograms recorded during the transit of the patch observed from 1006 to 1041 UT on January 22, 1982 (see Figures 1*a–c*) is shown in Figure 3. Figure 3*b* shows the subionograms with negative Doppler shift (from receding structures), and Figure 3*c* shows those with positive Doppler shift (from approaching structures). The ionograms in Figures 3 and 4 show a quasi-analog presentation of the Doppler shift associated with each echo, instead of the more commonly used echo amplitude. Low Doppler shifts appear as light grey, and high Doppler shifts appear darker [*Patenaude et al.*, 1973]. The sequence of ionograms shown is typical for the approach of an ionization patch and its transit through the zenith. Figure 3*a* shows the corresponding 6300-Å ASIP images, with the noon-midnight meridian aligned along the left horizon. The 1006 UT image shows, as discussed in section 2.1, the high latitude edge of the auroral oval in the 06–10 CGLT sector on the sunward horizon. A patch (hereinafter called patch A) moved out of that region in the antisunward direction. The leading edge arrived in the zenith at ~1021 UT; by 1036 UT the trailing edge of the patch was just crossing the zenith. In the last image taken at 1041 UT, the patch had moved approximately halfway out of the field of view toward midnight.

The positive Doppler ionogram at 1006 UT shows a typical low density nighttime F region with an $f_0F_2 \approx 2.8$ MHz (corresponding to N_e max $= 9.7 \times 10^4$ el cm^{-3}). The small area of high Doppler shift between 4.2 and 5.8 MHz, starting at a range of ~210 km are rangefolded returns from a reflecting/scattering structure at a virtual range of approximately 960 km. Since the sounder operated at a pulse repetition frequency of 200 Hz, returns from ranges larger than 750 km are rangefolded into the primary 750-km range. Phase coding of the transmitted HF signals and proper decoding in the receiver rejects all but very strong overrange echoes. This overrange return is the first indication of the approaching ionization patch. The ionograms taken at 1011 and 1021 UT clearly show the ionospheric signatures of the rapidly approaching patch. At 1011 UT high-Doppler returns are observed in the positive-Doppler ionogram at ranges ≥ 460 km. By 1021 UT the leading edge of patch A has reached the zenith. This is determined from the low-frequency trace ($f_0F_2 \sim 4$ MHz, N_e max $= 2.0 \times 10^5$ el cm^{-3}) observed at essentialy zero Doppler in both the positive and negative sub-ionograms. The heavy spread F trace with high positive Doppler, which is simultaneously observed at 1021 UT suggests that the major part of the patch is still approaching. This is clearly supported by the 1021 UT ASIP image, which shows a 6300-Å substructure in the zenith at the edge of a large approaching airglow region.

By 1036 UT, this airglow region (patch A) has almost completely passed through the zenith and the corresponding ionogram shows most of the ionospheric returns with strong negative Doppler. However, the signature of the ionization in the trailing region of the patch produces a clear virtual height trace in the ionogram with low positive Doppler and an $f_0F_2 = 8.0$ MHz (N_e max $= 8 \times 10^5$ el cm^{-3}). Since the echo amplitudes from overhead and slightly off-vertical regions differ very little, the overhead traces could only be identified by using their Doppler signatures. Finally, the ionogram at 1041 UT now shows all returns appearing in the negaitve Doppler ionogram at ranges ≥ 390 km. This suggests that the ionization patch has moved away from the zenith, as observed in the corresponding ASIP image. The weak trace (low Doppler) in the negative Doppler ionogram shows the low density overhead ionosphere with $f_0F_2 < 3$ MHz.

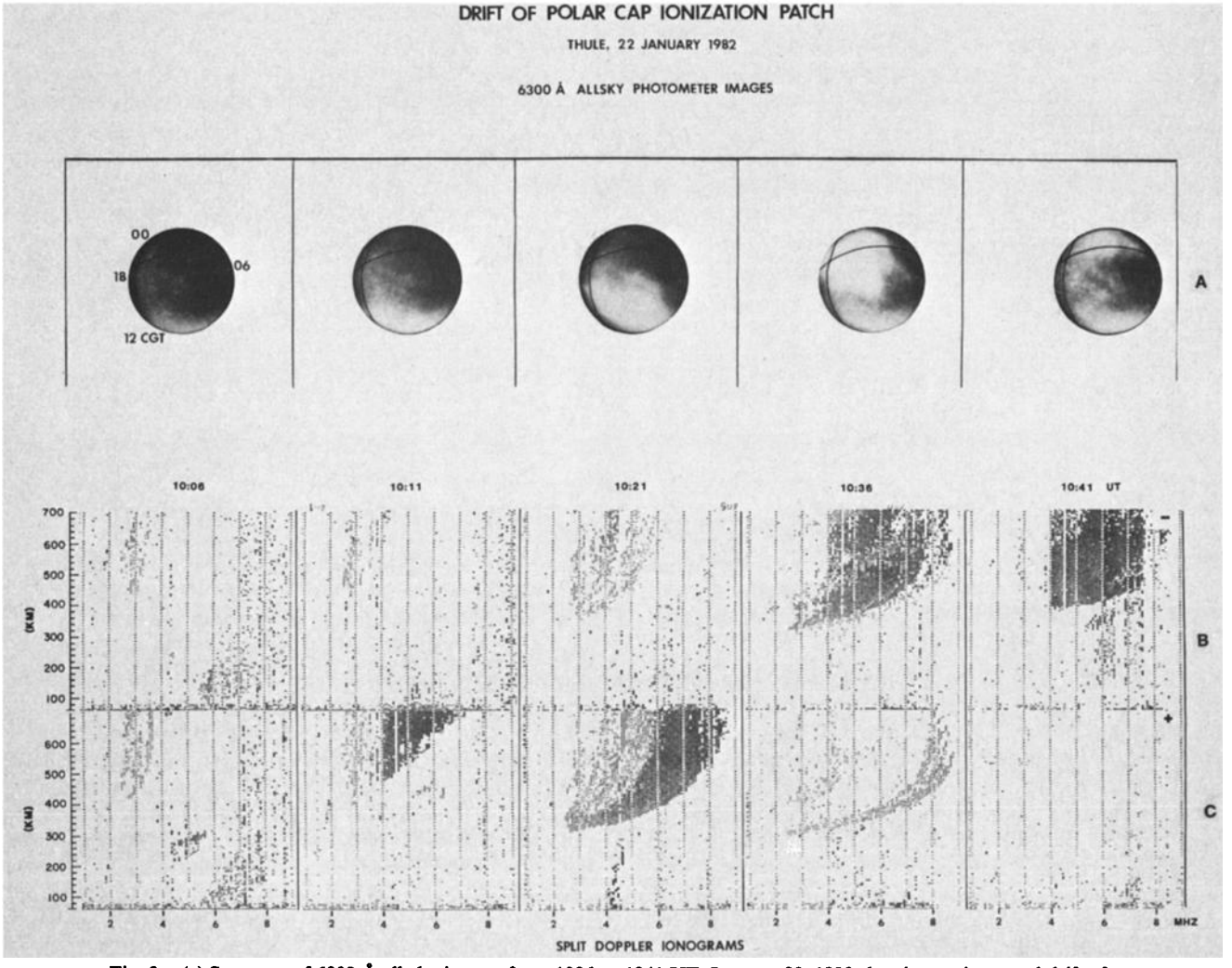

Fig. 3. (*a*) Sequence of 6300-Å all-sky images from 1006 to 1041 UT, January 22, 1982 showing antisunward drift of an airglow patch; (*b*) corresponding negative Doppler; and (*c*) positive Doppler Digital ionograms to illustrate *F* layer ionization characteristics associated with the patch.

The approach of the next patch (patch B) is shown in Figures 4*a*–*c*. The ASIP images (Figure 4*a*) show patch A low on the midnight horizon at 1046 UT and a new patch (patch B) moving out of the noon sector. By 1101 UT, the leading substructure of patch B arrived in the zenith, and by 1111 UT, patch B was centered over the station. The ionogram at 1046 UT shows the rapidly disappearing patch A visible in Figure 3*c*. The overhead ionosphere is again very weak ($f_0F_2 \approx 3.0$ MHz). At 1056 UT, patch A had moved out of the range of the ionosonde (and out of the field of view of the ASIP), while strongly enhanced and spread returns from patch B approach. By 1101 UT, the leading edge of patch B with an $f_0F_2 \approx 4$ MHz is overhead, and the ionogram at 1106 UT shows evidence of strong electron density enhancement ($f_0F_2 \approx 8$ MHz) in the negative Doppler panel. By 1111 UT, no distinct traces are obtainable, even though cusp-type structures in both the negative and positive Doppler ionograms indicate the presence of strongly enhanced and structured ionization in patch B, which is now in the zenith. It should be pointed out here, that the ability to separate signatures of ionospheric profiles or structures is most effective close to the leading or trailing edge of patches. In this case, most of the echo returns from the larger patch structure are separated from the signature of the overhead ionization by different Doppler shifts.

To establish the two-dimensional structure of a patch, a sequence of clearly identifiable ionogram traces was taken from all ionograms recorded during the transit of patch A up to the arrival of the leading edge of patch B. True height analysis was performed by using these traces. Since no *E* region returns were observed during this period, the starting height of the ionization was set at 180 km. An upper limit for the ionization density at *E* region heights can be set at $\leq 10^4$ el cm^{-3}, based on a combined assessment of the ionograms, the measured particle precipitation, and the 3914 Å N_2^+ zenith measurements. Setting this low *E* region density to zero for the true height analysis only slightly affects the resulting *F* region profiles and has no substantial impact on our conclusions.

Constant electron density contours along the noon-midnight axis of patch A are shown in Figure 5. The sequence of ASIP images indicated a horizontal velocity of $\sim$700 m s^{-1}. This is in good agreement with the ionization patch velocity of 700 to 780 m s^{-1} determined from the Doppler measurements. Since the ionosonde measures Doppler shift, i.e., the radial velocity component, more exact velocity measurements require knowledge of the height of the scattering or reflecting region and the exact raypath. Using a velocity of 700 m s^{-1}, the spacing of the ionograms in the horizontal

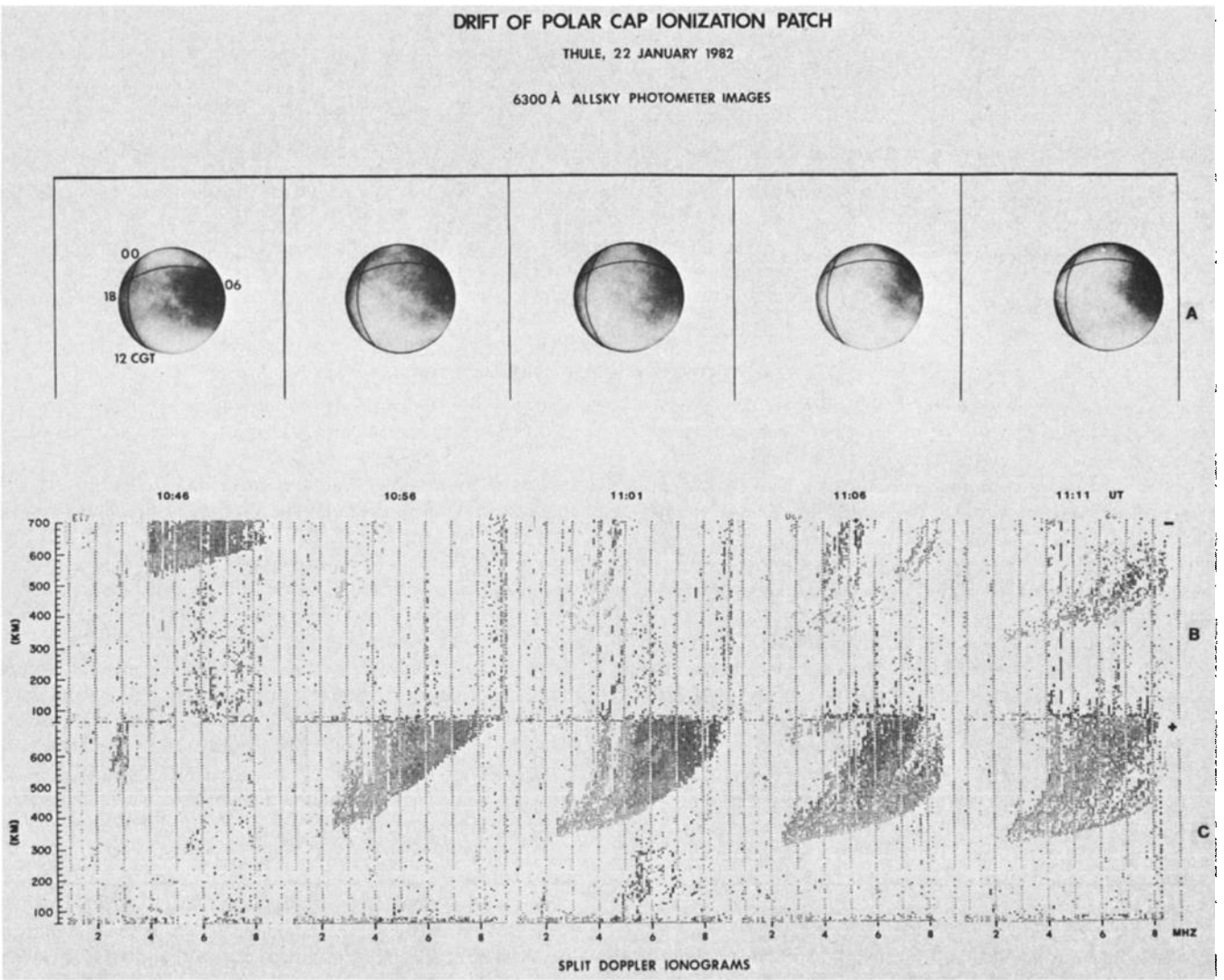

Fig. 4. Same as Figure 3 from 1046 to 1111 UT, January 22, 1982.

direction could be determined. They are indicated by the respective UT markers above the abscissa. It should be noted that the abscissa has twice the resolution of the ordinate. The heavy dots on the equidensity contours are computed values obtained from the true height analysis, the open circles represent the height of N_e max, the maximum density of the F layer patch at this location. A topside profile using a modified Chapman layer [*Tinsley et al.*, 1973] has been matched to each bottomside profile, to provide the necessary input to the computation of the 6300-Åemission in section 2.3.

The resulting cross-section shows a localized eightfold enhancement of electron density above the background ionization of $\leq 10^5$ el cm^{-3}. The horizontal dimension is $\sim$1200 km. The leading edge of the patch has a horizontal gradient scale length $L \geq 230$ km, where $L \equiv [(1/N)\,(\partial N/\partial X)]^{-1}$ while the trailing edge is steeper ($L \approx 100$ km). The dashed section of the bottomside contours between 1036 and 1046 UT indicates uncertainty of the exact profiles in this region. There is some indication that the ionization drops well below the 1.1×10^5 el cm^{-3} measured at 1046 UT and therefore the N_e gradient on the trailing edge might be considerably larger. The figure also shows the leading edge of patch B.

The transit of a patch at a velocity of 700 m s^{-1} leads to rapid changes in the observed minimum virtual range or height (h') from overhead and oblique returns in the ionogram. The integrated height characteristic shown in Figure 6, produced by collapsing each amplitude ionogram onto its height axis, permits a quick survey of the h' variation over extended

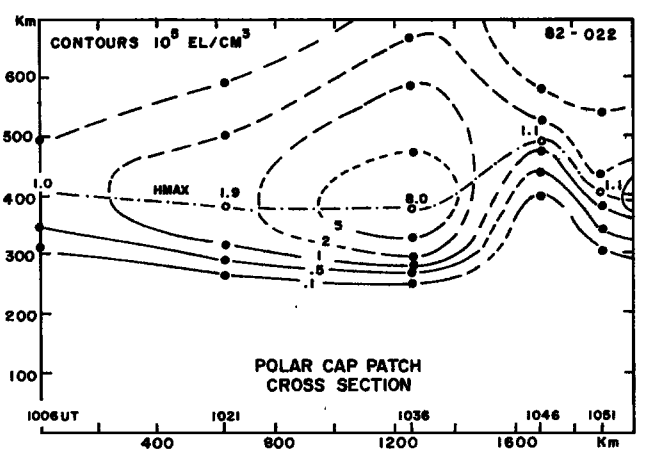

Fig. 5. Electron density contours along the noon-midnight axis of the ionization patch observed from 1006 to 1051 UT. The horizontal scale was determined by using the measured drift velocity of 700 m s^{-1}.

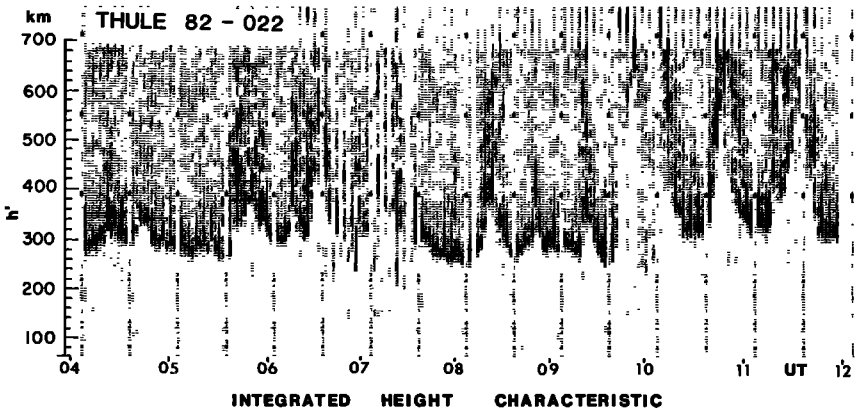

Fig. 6. Virtual height/range characteristics using both positive and negative Doppler ionograms for January 22, 1982.

periods. Figure 6 contains approximately 200 ionograms for eight hours of observations. The lower boundary of the heavy, dark trace represents $h'(t)$, which changes by as much as 400 km in 15 min. These fast transitions are the signatures of the strongly enhanced ionization patches moving rapidly in a background of very low density. The optical patches reported in the zenith at 0806, 0933, 1030 (patch A), and 1112 UT (patch B) are easily identified in the integrated height characteristic. Especially patches A, B, and a last one that reached the zenith at ~1150 UT are individually identifiable over distances larger than 1000 km owing to their large separation. The slope of the range change during approach and retreat characterizes the bulk motion of the patch ionization and corresponds to velocities ≥ 600 m s^{-1}. These are in good agreement with the optical and Doppler measurements, considering that no refraction effects have been taken into account.

2.3. *Precipitating Particle Characteristics*

Precipitating particle measurements from the low-altitude plasma instrument (LAPI) on Dynamics Explorer 2 were available for January 22, 1982, from passes in the vicinity of Thule at 0655, 0831, and 1007 UT for comparison with the ground-based measurements. The 0655 UT pass was within 109 km of Thule and enables a direct comparison between particle fluxes and optical emissions. Plate 1 shows the differential energy flux, in spectrogram form, for electrons and ions measured at 46° pitch angle. (Note: Plate 1 is shown in the separate color section of the journal.) From these data, the polar cap is easily recognized on the spectrogram between 0652:25 UT (78.4° Λ, 0300 MLT) and 0701:00 UT (74.8° Λ, 1430 MLT). In this region only soft electrons are observed. Their spectral peak energy is ~100 eV.

The ASIP 6300-Å image at 0654 UT is shown in Figure 7. To compare the particle and optical data, the satellite position at each half minute, beginning with 0652:30 UT, was traced downward by using the 1980 IGRF model from the satellite altitude (735–790 km) to an approximate loss height of 250 km. These positions were then plotted into the ASIP image. The numbers 1–9 in the ASIP image correspond to the same numbers in the spectrogram. Although the polar cap precipitation is not completely uniform, the small variations do not correspond to the ~1000-km scale size of the patches seen in the 6300-Å image.

This comparison suggests that the localized 6300-Å patches seen in the ASIP images and in the intensity variations in Figure 2 are not produced by direct particle precipitation but are primarily airglow structures produced by patches of enhanced F region ionization. The motion of the features suggests that this ionization was not locally produced but is observed after production as it convects across the polar cap in the antisunward direction. During the period of observation, this ionized patch undergoes chemical recombination that results in the 6300-Å airglow.

To test this hypothesis, the total 6300-Å emission (direct excitation from precipitating electrons plus airglow from dissociative recombination) has been estimated for patches near the aircraft zenith during the DE passes at 0655 and 1007 UT. The quantitative behavior of these patches is clearly seen in the 6300-Å intensity measurements in Figure 2. The first patch under consideration drifted through the spectrometer field of view from 0640 to 0712 UT, the second patch from 1018 to 1040 UT.

First patch. The electron spectra at 0655:27 UT (Figure 8) were used to calculate the contribution from the polar rain and from photoelectrons produced below the satellite. For the polar rain contributions, spectra were averaged over the 62° loss cone using detectors at 9°, 46°, and 61°. The photoelectrons, such as those described by *Winningham and Gurgiolo* [1982], are produced by scattered UV radiation below the satellite and are distributed isotropically. They are detected at satellite altitude in the upcoming (136° pitch angle) detectors at energies between 5 and ~60 eV. Since they are isotropic, similar fluxes are expected to precipitate into the F layer and contribute to 6300-Å emission. The polar rain and photoelectron fluxes of Figure 8 have been added to obtain an effective spectrum representing the total particle flux incident on the F layer. The auroral ionization/emission model (D. J. Strickland, private communication, 1983), based on the electron transport code of *Strickland et al.* [1976], was used to calculate the expected 6300-Å emission and the electron density profile from the incident spectrum. The calculated value of 70 R is shown as a base level in Figure 2, since the polar rain fluxes did not show significant spatial variation in the vicinity of Thule.

The airglow contribution was calculated by using true height bottomside profiles from the digital ionograms [*Reinisch and Huang*, 1983]. These were matched at the F layer peak to a modified Chapman function [*Tinsley et al.*, 1973], to extend the profile above the peak to 650 km. The calculation of the 6300-Å airglow from charge exchange of O^+ with O_2, followed by dissociative recombination of O_2^+ is identical to the method outlined in the work of *Weber et al.* [1982].

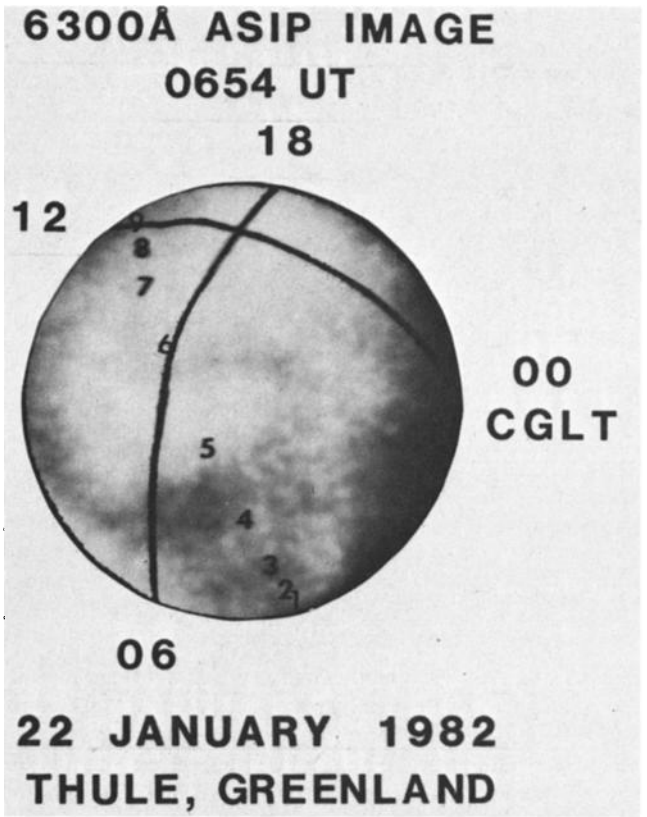

Fig. 7. All-sky imaging photometer (ASIP) image at 0654 UT. The numbers 1–9 in the ASIP image are the positions of the magnetic field line traced from satellite altitudes down to the 250 km interaction height.

Airglow intensities were calculated whenever a reliable true height profile could be derived from the ionogram. Spread F at other times precludes the derivation of true height profiles. The calculated airglow plus precipitating electron contributions (open circles) are shown in Figure 2. These agree to within 30 R of the measured values both within and outside the patch. This comparison indicates that the background level of 6300-Å emission is due to precipitating electrons, and the increases above background are due to airglow production within the high-density patches. Although the electron spectrum can account for the 6300-Å emission outside the patch, the ionization production (and resulting electron density profile) from this spectrum is not sufficient to account for the measured electron density in the background ionosphere. Figure 9 shows electron density profiles derived from the ionograms inside and outside the patch. Also shown is the electron density profile from the numerical code using the composite spectrum in Figure 8. The measured background density is almost one order of magnitude larger, and the layer peak is found at higher altitudes than the profile resulting from the numerical calculation and shows that local fluxes are not sufficient to produce the measured polar *F* layer density. This suggests that the entire observed ionosphere (patches plus background) is transported into the polar cap from a source region within or equatorward of the dayside auroral zone.

Second patch. The energy time spectrogram for electrons at pitch angels of 46° and 136° on the 1007 UT pass is shown in Plate 2. (Note: Plate 2 is shown in the separate color section of the journal.) As was the case during the 0655 UT pass, the polar cap electron precipitation is unstructured and low in energy. Since the satellite passed 880 km to the west of Thule on this pass, direct comparison within a common ionospheric volume was not possible. In an attempt to represent accurately the fluxes at Thule, the polar rain spectrum was selected at a time when the satellite was nearest Thule's geomagnetic latitude (1009:00 UT, Plate 2); but the photoelectron spectrum was selected at a time when the shadow height at the satellite location was 800 km, the same as that above Thule (this occurs at 1011:00 UT in Plate 2). These spectra are shown in Figure 8, and as in the 0655 UT pass, they have been added to obtain an effective spectrum incident on the *F* layer. When used in the ionization/emission code, the result is a calculated value of 6300-Å emission of 92 R. This is in good agreement with the observed value of 100 R outside the patch and suggests little spatial variation in the polar rain between Thule and the DE field line.

Calculation of the airglow component of this patch used the true height profiles shown in Figure 5. Since the calculated and measured background intensity differ slightly, we used the locally measured value of 100 R as a baseline and added the calculated airglow intensity to this. These are shown as open circles in Figure 2 for the patch near the zenith from 1017 to 1040 UT. Using the 100 R background, the calculated airglow values show excellent agreement with the measured intensities.

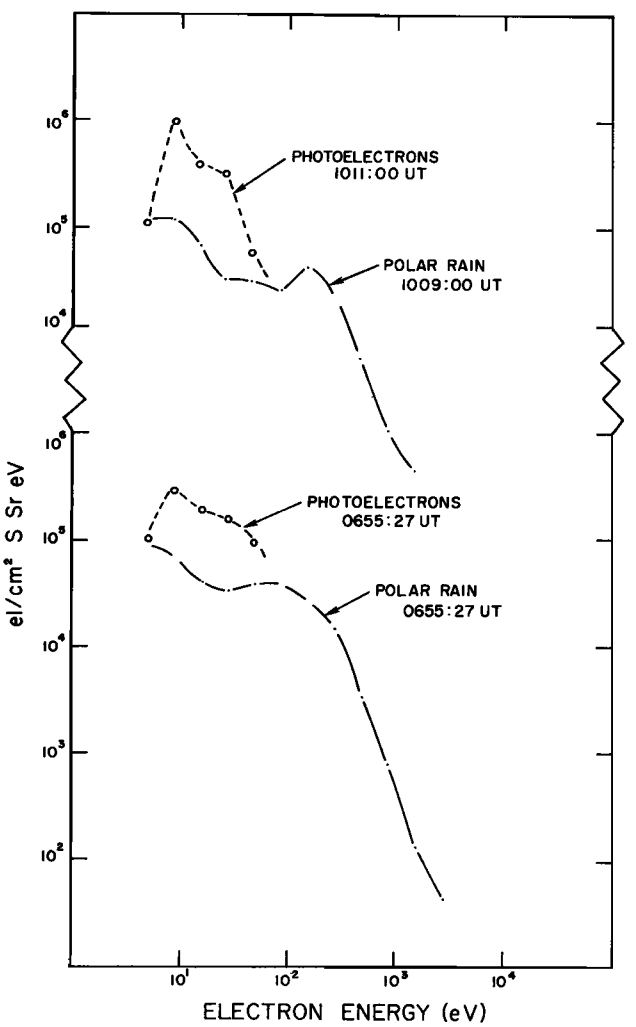

Fig. 8. Electron sources of 6300-Å emission and *F* layer ionization showing polar rain and photoelectron spectra at the nearest approaches of the subsatellite point to Thule during the 0655 UT and 1007 UT passes.

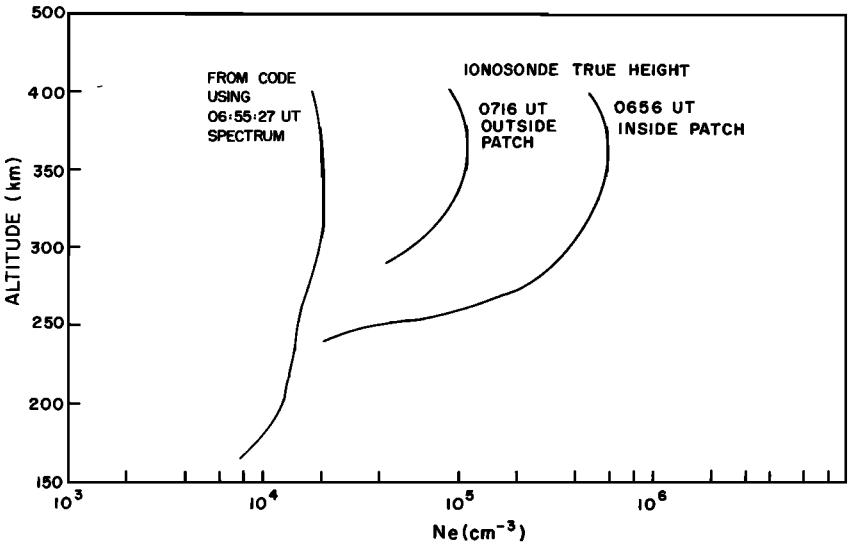

Fig. 9. Electron density profiles inside and outside *F* layer patch determined from true height analysis of ionograms. Also shown is the profile expected from soft electron precipitation into the polar cap.

These comparisons of LAPI data with measured airglow and electron densities confirm that the ionization patches are not locally produced but are transported into the polar cap from a source region upstream in the $E \times B$ convective flow pattern. In addition, the polar rain fluxes are not sufficient to account for production of the background ionization between the patches. This plasma, therefore, must also be transported into the polar cap. Possible source regions are discussed in section 3.

2.4. *Intermediate Scale Structure*

The large-scale patches seen optically and with the sounder are subject to instability processes that will produce intermediate scale (few kilometers and smaller) irregularities. To characterize these secondarily produced irregularities, complex signal radiowave scintillation measurements were made throughout the January 21–27 period. The signal sources for these observations were polar orbiting beacons in highly eccentric orbits, which transmit at 250 MHz. These appear at high elevation angles for extended periods over Thule and provide near-continuous raypath penetrations through the central polar cap *F* region. The information provided by the complex signal data includes the irregularity strength at spatial scales from a few kilometers to about 100 m [*Rino*, 1982] and, through the use of spaced receivers, the irregularity anisotropy and drift [*Rino and Livingston*, 1982]. Thus we can establish the spatial association between the irregularities and the macroscale patches, and determine their relative motion.

The measured signal intensity scintillation index S_4 is plotted in Figure 10 for the period of interest. It is a good first-order indicator of irregularity occurrence, and comparison with the raypath penetration points shown by dots in Figure 1*a–c*, shows that there is a clear association between the patches and kilometer scale structure. When the raypath passes through the high density patches, the S_4 index approaches saturation ($S_4 \sim 1$), while the intervening low-density regions produce only weak signal variations. To illustrate this correlation more clearly, times when four major optical patches intersected the satellite raypath between 0700 and 1200 UT are indicated on Figure 10*a*.

The complex signal data makes it possible to obtain, additionally, a measure of the absolute density turbulence in the patches. This is because the signal phase provides a near-direct mapping of the irregularity continuum for the scintillation conditions of interest in this case [*Rino*, 1982]. The turbulence estimates are made by using phase scintillation spectral parameters, as outlined in the work of *Livingston et al.* [1981], and the irregularity anisotropy and drift, which are measured directly by using spaced receivers [*Rino and Livingston*, 1982]. The resulting estimate of three-dimensional turbulent strength C_s is shown in Figure 10*b*. The S_4 index and C_s generally track, as they must, but C_s provides a measure of the true dynamic range of the density turbulence. For example, if we assume a constant irregularity layer thickness, the structuring or turbulence on the sunward edges of the patches is some 30 dB stronger than that in the low-density background regions. It is interesting to note that the peak C_s levels in Figure 10*b* correspond to median levels observed at the magnetic equator during moderate sunspot conditions [*Livingston et al.*, 1981].

The data in Figure 10*a* also provide information about the instability mechanism that is producing the kilometer scale structure. The first, third, and fourth patches, i.e., those isolated and clearly defined, show a systematic difference in the severity of scintillation on their leading and trailing edges. The scintillation produced by irregularities within the trailing (sunward) edge always exceeds that produced by irregularities with the leading (antisunward) edge. This asymmetry compares well with the electron density contours determined from the ionograms (Figure 5), and with the zenith 6300-Å intensities that show a slow rise followed by a steep drop (Figure 2). Combined, these observations suggest that it is the gradient drift instability [*Linson and Workman*, 1970] that produces the secondary structuring within the patches.

The irregularity drift during this same period as measured by the spaced receiver method is shown in Figure 11. The motion is antisunward, with a small component toward the dawn sector. During the passage of the 1020 UT patch through the line of sight, the velocity is about 600 m s^{-1}, in good agreement with the drift velocity of the overall patch estimated from optical and sounder measurements. There is a general increase in the velocity between dawn and noon at these latitudes, in agreement with the models of two-celled convective plasma flow in the polar cap [*Heelis et al.*, 1982].

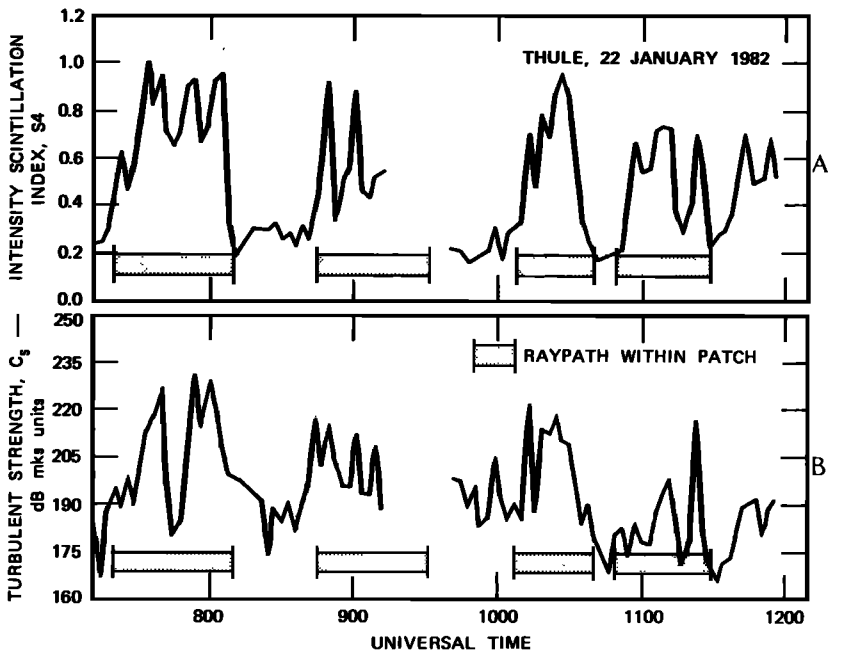

Fig. 10. Scintillation parameter (S_4) and irregularity turbulence strength (C_s) for January 22, 1982. Times when the signal raypath was within an F region patch are indicated.

Drift of the neutral atmosphere, which results primarily from ion drag at this season and latitude, will follow the same flow pattern, but will lag the plasma by an hour or more. The result, in the morning sector, is that the antisunward plasma flow will be more rapid than the neutral flow. As discussed by *Linson and Workman* [1970] for barium cloud striations, irregularity generation is expected in regions where the ion drift velocity vector and electron density gradient are parallel. In the reference frame of the neutrals, therefore, it is the sunward edge of the patches that are gradient drift unstable; here the drift and gradient vectors are parallel, resulting in steepening and eventual structuring. Using the measured parameters of $V_{patch} = 700$ m s^{-1}, $L = 100$ km and an expected neutral wind speed between $V_n = 100$–200 m s^{-1} in the antisunward direction [*Roble et al.*, 1982] gives a growth time $\tau(L/V_{patch} - V_{neutral})$ of ~170–208 s near the F layer peak on the trailing edge of this patch. Although the trailing edge of the patch contains the most intense irregularities, the entire patch structure is populated with kilometer-scale irregularities of sufficient intensity to produce saturated UHF amplitude scintillation. This is to be expected since the gradient drift mechanisms will eventually structure a large fraction of the original patch.

3. Conclusions

Coordinated ionospheric measurements have shown the existence of large patches of enhanced ionization drifting across the polar cap in the antisunward direction during moderately disturbed ($Kp \geq 4$) geomagnetic conditions. The patches (~ 800–1000 km diameter) were initially observed as they separated from the morning sector of the auroral oval. Drift speeds ranged from 500 to 1000 m s^{-1} corresponding to a dawn-dusk electric field strength of 25–50 mV m^{-1}. Simultaneous Dynamics Explorer 2 LAPI measurements show no direct precipitating particle source for these regions of increased ionization. In addition, the polar rain fluxes are not sufficient to produce the background densities observed between the patches. This comparison suggests that all of the polar cap ionization (patch plus background) was produced further upstream in the high-latitude convection flow pattern. Possible source regions include ionization produced in the sunlit ionosphere and transported into the polar cap by $\bar{E} \times \bar{B}$ drift.

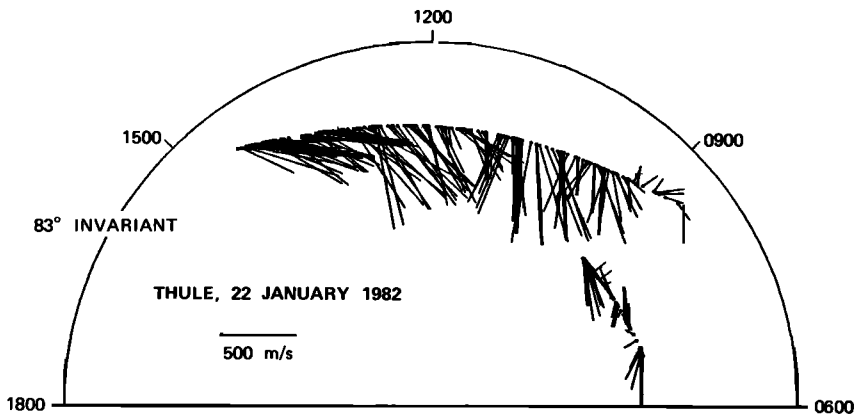

Fig. 11. CG latitude/local time plot showing irregularity drift pattern determined from spaced receiver scintillation measurements.

Another possibility is a source region associated with convection through the dayside aurora/cusp precipitation region. In either case, the source region and transport mechanism must account for the nonuniform distribution of plasma and the high peak density (10^6 cm^{-3}). Steady convection through the cusp region, for example, would not produce the discrete patches seen in the polar cap. Estimates made by *Knudsen* [1974] indicate that direct convection through the cusp would add $\sim 2 \times 10^5$ el cm^{-3} to the density near the peak of the F layer. This may be a source for the background polar F layer, which has a density comparable to that expected from the cusp. Direct convection through the cusp, however, does not result in the large densities observed in the patches. A possible mechanism would be sunward convection along the cusp for tens of minutes before the antisunward flow across the polar cap. This "spatial resonance" would allow sufficient time for the electron density to build up to $\sim 10^6$ el cm^{-3}. Alternatively, spatial/temporal variations in the high-latitude electric field may periodically attach solar produced sub-oval (corotating) plasma ($N_{max} \sim 10^6$ el cm^{-3}) to the $E \times B$ convective flow system. Subsequent drift would then be controlled by high-latitude convection. Further experiments are clearly needed to identify the source region of the patches. Also, future experiments are needed to investigate the relation of the polar cap patches to F region ionization enhancements observed near the nightside auroral zone with the Chatanika radar [*Vickrey et al.*, 1980].

Time evolution of the patch leads to a steepening of the trailing edge and to the generation (or possible restructuring) of ionospheric irregularities. A distinct asymmetry is noted in irregularity intensity on the leading and trailing edges. The patch geometry and drift direction suggests that this asymmetry could be a result of the $E \times B$ instability.

The ionosonde measurements provide an approximate cross-section through the polar cap F region patches along the axis of this motion. Bulk velocity and instantaneous Doppler measurements show a velocity of 600–750 m s^{-1}, in good agreement with the optical measurements. The patches with peak density of 10^6 el cm^{-3} are observed in a weak background ionization (N_e max $\leq 10^5$ el cm^{-3}). The leading edges of these patches have a considerably weaker horizontal N_e gradient than the trailing edges. During the occurrence of these patches under moderately disturbed geomagnetic conditions no E region ionization was observed.

Acknowledgments. The authors wish to thank R. W. Gowell, J. W. F. Lloyd, and J. B. Waaramaa of AFGL for engineering support and M. Shirley of the University of Lowell and W. Whiting of Regis College for analysis support. Assistance with the auroral ionization/emission code was generously provided by D. J. Strickland. The support and cooperation of the flight crew and ground personnel of the 4950th TW, AFSC, Wright-Patterson Air Force Base, Dayton, Ohio, is gratefully acknowledged. This research was supported in part by the following contracts: DNA S99QAXHC WU20/21 (AFGL), AFGL F19628-80-C-0064 (University of Lowell), NASA NAS 5-26363 and AFGL FY712183N0001 (SWRI), and AFGL under Sandia 55-3136 (SRI).

The Editor thanks D. Strickland and M. C. Kelley for their assistance in evaluating this paper.

REFERENCES

Aarons, J., J. P. Mullen, H. E. Whitney, A. L. Johnson, and E. J. Weber, UHF scintillation over polar latitudes, *Geophys. Res. Lett.*, *8*, 277, 1981.

Bibl, K., and B. W. Reinisch, The universal digital ionosonde, *Radio Sci.*, *13*, 519, 1978.

Buchau, J., B. W. Reinisch, E. J. Weber, and J. G. Moore, Structure and dynamics of the winter polar cap F region, *Radio Sci.*, *18*, 995, 1983.

Gussenhoven, M. S., Extremely high latitude auroras, *J. Geophys. Res.*, *87*, 2401, 1982.

Hardy, D. A., Intense fluxes of low-energy electrons above the auroral oval and in the polar cap, *J. Geophys. Res.*, *88*, in press, 1983.

Heelis, R. A., and W. B. Hanson, High latitude ion convection in the nighttime F region, *J. Geophys. Res.*, *85*, 1995, 1980.

Heelis, R. A., J. A. Lowell, and R. W. Spiro, A model of the high-latitude ionospheric convection pattern, *J. Geophys. Res.*, *87*, 6339, 1982.

Heppner, J. P., Electric field variations during substorms: OGO 6 measurements, *Planet. Space Sci.*, *20*, 1475, 1972.

Kelley, M. C., J. F. Vickery, C. W. Carlson, and R. Torbert, On the origin and spatial extent of high-latitude F region irregularities, *J. Geophys. Res.*, *87*, 4469, 1982.

Knudsen, W. C., Magnetospheric convection and the high latitude F_2 ionosphere, *J. Geophys. Res.*, *79*, 1046, 1974.

Lassen, K., and C. Danielsen, Quiet time pattern of auroral arcs for different directions of the interplanetary magnetic field in the y-z plane, *J. Geophys. Res.*, *83*, 5277, 1978.

Linson, L. M., and J. B. Workman, Formation of striations in ionospheric plasma clouds, *J. Geophys. Res.*, *75*, 3211, 1970.

Livingston, R. C., C. L. Rino, J. P. McClure, and W. D. Hanson, Spectral characteristics of medium-scale equatorial F region irregularities, *J. Geophys. Res.*, *86*, 2421, 1981.

Maezawa, K., Dependence of geomagnetic activity on solar wind parameters: A statistical approach, *Solar Terr. Environ. Res.* Jpn., *2*, 103, 1978.

Patenaud, J., K. Bibl, and B. W. Reinisch, Direct digital graphics, *Am. Lab.*, *15*, 95, 1973.

Reinisch, B. W., and Huang Xueqin, Automatic calculation of electron density profiles from digital ionograms, 3, Processing of bottomside ionograms, *Radio Sci.*, *18*, 477–492, 1983.

Rino, C. L., On the application of phase screen models to interpretation of ionospheric scintillation data, *Radio Sci.*, *17*, 855, 1982.

Rino, C. L., and R. C. Livingston, On the analysis and interpretation of spaced receiver measurements of transionospheric radio waves, *Radio Sci.*, *17*, 845, 1982.

Roble, R. G., R. E. Dickinson, and E. C. Ridley, Global circulation and temperature structure of thermosphere with high-latitude plasma convection, *J. Geophys. Res.*, *87*, 1599, 1982.

Strickland, D. J., D. L. Book, T. P. Coffey, and J. A. Fedder, Transport equation techniques for the deposition of auroral electrons, *J. Geophys. Res.*, *81*, 2755, 1976.

Tinsley, B. A., A. B. Christensen, J. A. Bittencourt, P. D. Angreji, and H. Takahashi, Excitation of oxygen permitted line emissions in the tropical nightglow, *J, Geophys. Res.*, *78*, 1174, 1973.

Vickrey, J. F., C. L. Rino and R. A. Potemra, Chatanika/TRIAD observations of unstable ionization enhancements in the auroral F region, *Geophys. Res. Lett.*, *7*, 789, 1980.

Weber, E. J., and J. Buchau, Polar cap F layer auroras, *Geophys. Res. Lett.*, *8*, 125, 1981.

Weber, E. J., J. Buchau, R. H. Eather, and J. W. F. Lloyd, Large scale optical mapping of the ionosphere, *Rep. AFGL-TR-77-0236*, Air Force Geophys. Lab., Bedford, Mass., 1977.

Weber, E. J., H. C. Brinton, J. Buchau, and J. G. Moore, Coordinated airborne and satellite measurements of equatorial plasma depletions, *J. Geophys. Res.*, *87*, 10503, 1982.

Winningham, J. D., and C. Gurgiolo, DE-2 photoelectron measurements consistent with a large-scale parallel electric field over the polar cap, *Geophys. Res. Lett.*, *9*, 977, 1982.

Winningham, J. D., and W. J. Heikkila, Polar cap auroral electron fluxes observed with ISIS I, *J. Geophys. Res.*, *79*, 949, 1974.

J. Buchau, J. G. Moore, and E. J. Weber, Ionospheric Physics Branch, Air Force Geophysics Laboratory, Hanscom Air Force Base, MA 01731.

R. C. Livingston, Radio Physics Laboratory, SRI International, 333 Ravenswood Avenue, Menlo Park, CA 94025.

B. W. Reinisch, Center for Atmospheric Research, University of Lowell, Lowell MA 01854.

J. R. Sharber, Physics and Space Sciences Department, Florida Institute of Technology, Melbourne, FL 32901.

J. D. Winningham, Southwest Research Institute, P.O. Drawer 28510, San Antonio, TX 78284.

(Received July 7, 1983;
revised August 31, 1983;
accepted September 1, 1983.)

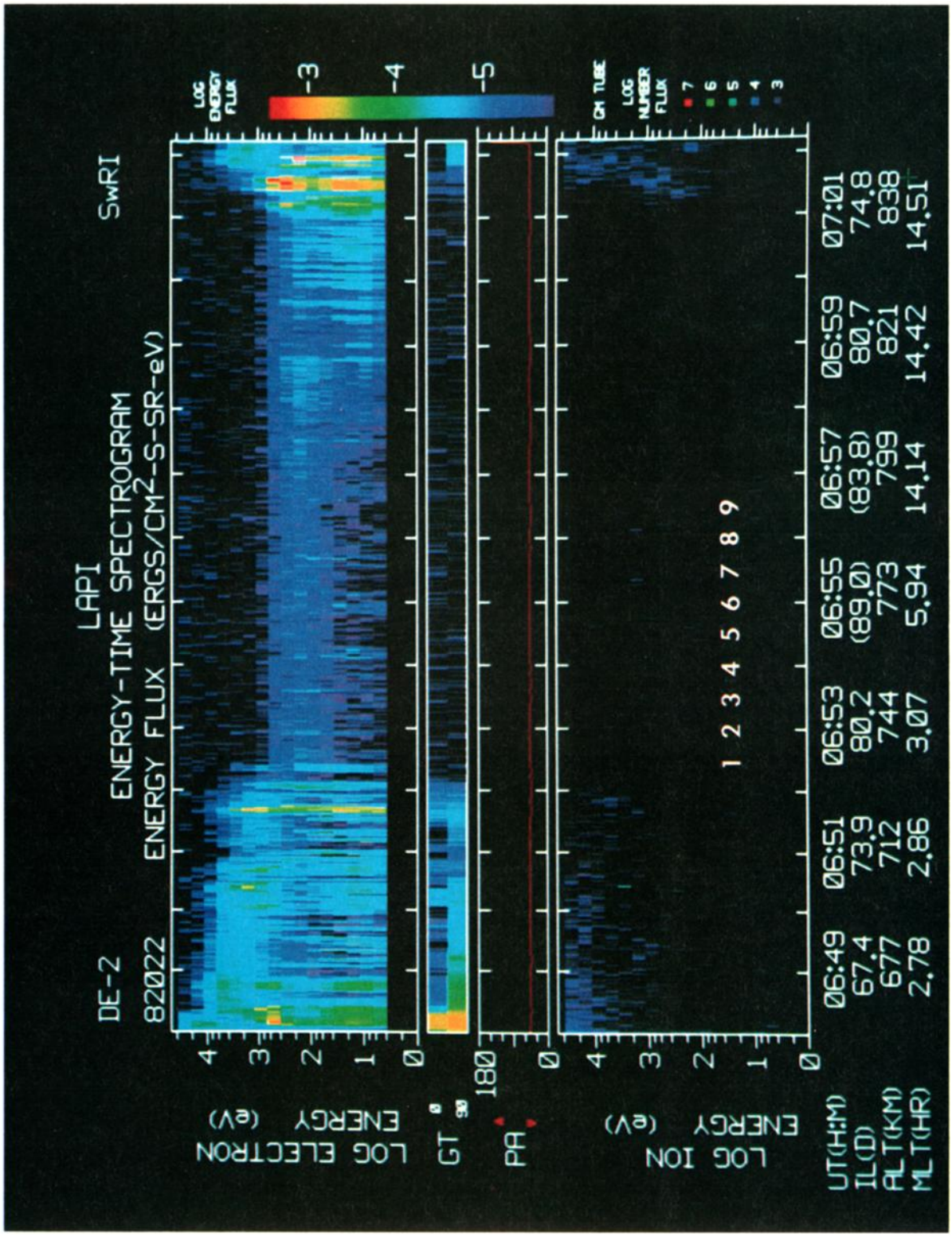

Plate 1 [*Weber et al.*]. 0655 UT pass of the dynamics Explorer 2 satellite over the northern polar cap on January 22, 1982, showing electrons and ions at 46° pitch angle and Geiger counter measurements of the low-altitude plasma instrument (LAPI). The polar cap lies between 0652:25 UT (78.4° Λ) and 0701:00 UT (74.8° Λ). The distance of closest approach of the subsatellite point to Thule was 109 km and occurred at 0654:37 UT.

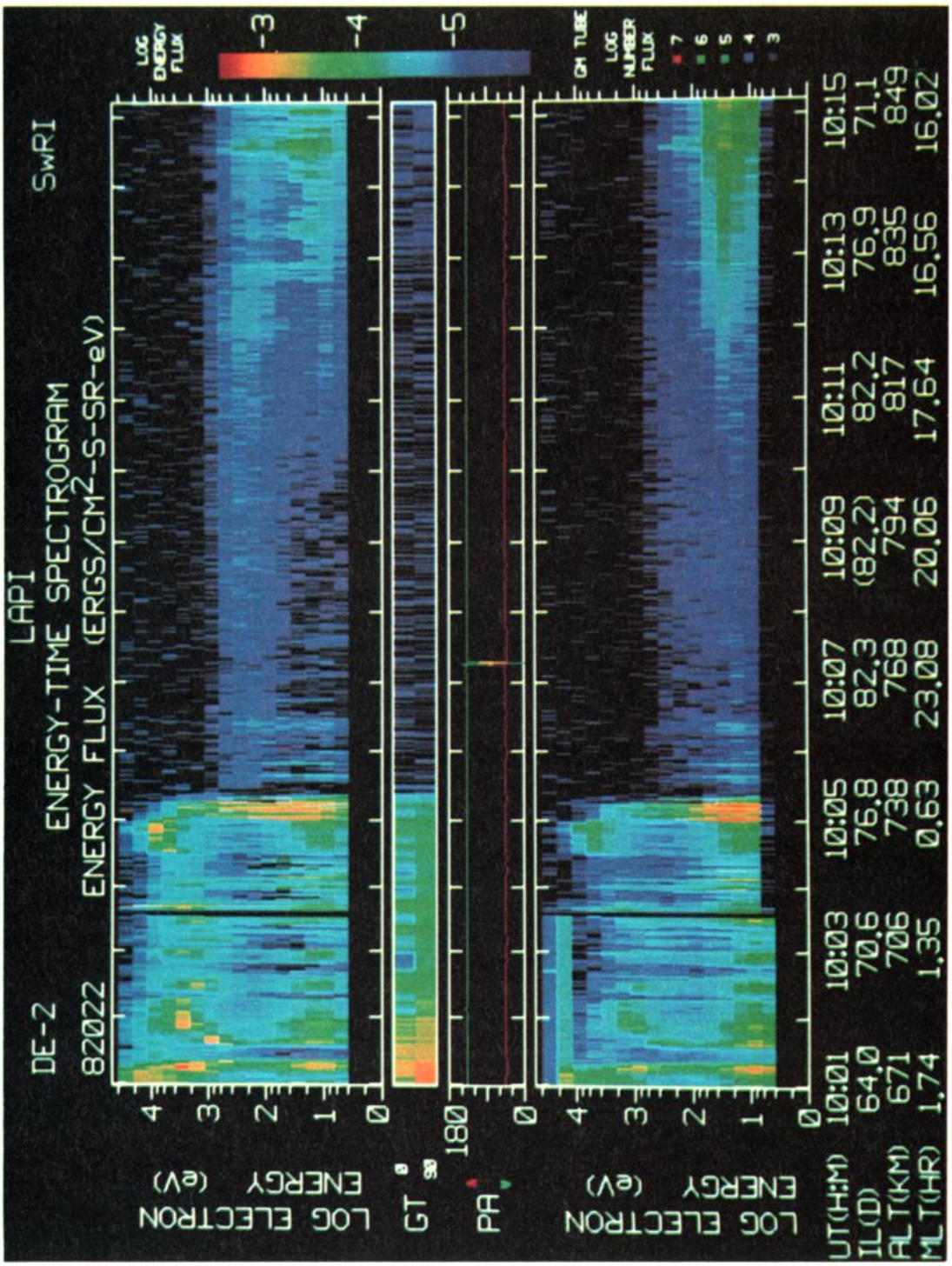

Plate 2 [*Weber et al.*]. 1007 UT pass of DE-2 over the northern polar cap on January 22, 1982. Upper and lower panels show LAPI measurements of downward electron fluxes at 46° pitch angle and upward electron fluxes at 136° pitch angle, respectively.